TURBULENT BOUNDARY LAYER SEPARATION - PASSIVE CONTROL

Ola Lögdberg
KTH Mechanics, Royal Institute of Technology
S-100 44 Stockhom, Sweden
ola@mech.kth.se

P. Henrik Alfredsson
KTH Mechanics, Royal Institute of Technology
S-100 44 Stockhom, Sweden
hal@mech.kth.se

ABSTRACT

We report results where a separated turbulent boundary layer is controlled using vortex generators of various heights. Measurements are performed using Particle Image Velocimetry (PIV) and velocity profiles, reversed flow profiles and integral parameters of the boundary layer are presented. The effectiveness of the separation control is shown to depend on the circulation induced by the vortex generators and for the largest values a complete cancellation of the separation seems to be possible.

INTRODUCTION

Control of separated flows is of interest in many applications, for instance on airplane wings, on vehicles (both cars and commercial vehicles) and in various internal flows. Many different types of control schemes, both passive and active have been proposed and tested (see e.g. Gad-el-Hak & Bushnell, 1991). For laminar separation bubbles both sound waves and free stream turbulence is known to force reattachment earlier than in the undisturbed case (Häggmark, 2000). Slot injection is another possibility for geometry induced separation. Various types of active control (micro-jets etc.) have also been tried (e.g. Lin et al., 1990, Glezer & Amitay, 2002).

In the the present work we are following in the steps of Angele and Muhammad-Klingmann (2005a) (AMK in the following) using vortex generators in order to control the separation. In contrast to their earlier work the separation is much stronger in the present case and we make a parametric study of several vortex generators showing for which parameters reattachment occurs and interpret the results in terms of the circulation induced by the vortex generators. We also show detailed measurements of the velocity field including the reverse flow parameter.

EXPERIMENTAL SETUP

Wind tunnel

The experiments were conducted in the BL wind tunnel at KTH Mechanics. The test section is 4.0 m long and has a cross sectional area of 0.75×0.5 m^2 (height×width). For a detailed description of the wind tunnel the reader is referred to Lindgren & Johansson (2002). A schematic of the experimental setup is shown in figure 1. A vertical flat test plate made of Plexiglas, which spans the whole height and length of the test section, is mounted with its upper surface 300 mm from the the back side wall of the test section. After 1.25 m the test section is diverged by using a flexible wall in order to decelerate the flow. Suction is applied on the flexible wall to prevent separation on the curved wall and induce an adverse pressure gradient (APG) on the test plate. The suction rate in this experiment was set to 12.5–13 % of the flow over the flat plate at the inlet of the test section. The free stream velocity at the inlet of the test section was 26.5 m/s. The temperature of the air can be held constant through a heat exchanger system and was kept at 22 °C.

Pressure gradient

In figure 2 the pressure coefficient

$$C_p = \frac{P - P_{ref}}{P_0 - P_{ref}} \tag{1}$$

for the wall static pressure (P) and its gradient in the flow direction are plotted against the distance from the leading edge of the test plate. P_{ref} is taken on the wall at $x = 0.45$ m and P_0 is the total pressure at the same x position.

PIV equipment

The PIV-system used consists of a 400 mJ double cavity Nd:Yag laser operating at 15 Hz and a 1018×1008 pixels CCD camera with 8 bit resolution. The air was seeded with smoke droplets generated by heating glycol and injected in the pressure equalizer slit downstream of the test section.

Conventional post-processing validation procedures were used. No particles moving more than 25 % of the interrogation area length were allowed in order to reduce loss-of-pairs and the resulting zero-velocity bias. The peak height ratio between the highest and the second highest peak in the correlation plane must be more than 1.2 if the vector should be kept. Using these criteria on the data resulted in a validation rate of more than 95 % for the measurements at $x = 2500$ mm.

The images are all approximately 90×90 mm^2. Using 32×32 pixels interrogation areas the spatial resolution is 2.8 mm. The time between the cross-correlated image pairs was 30–35 μs. This makes the ratio between the discretization velocity u_d and the *rms* value of the streamwise velocity less than 2. According to AMK (2005b) this reduces errors due to peak-locking effects in mean and *rms* values to less than 1 %.

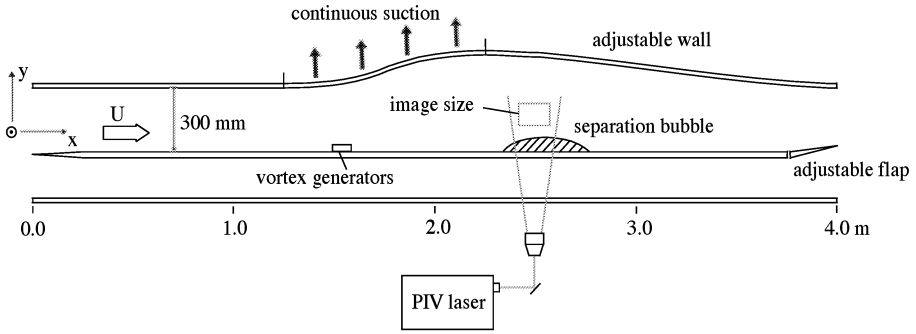

Figure 1: Schematic of the experimental setup.

In order to be able to obtain velocity data for the full height of the boundary layer images were taken at two different positions in the normal direction at each x–station. To follow the uncontrolled boundary layer development measurements were made at eleven different x–stations. Typically 1024 or 2048 image pairs were taken at each position.

UNCONTROLLED CASE

Velocity profiles

Figure 3 shows six mean velocity profiles between x = 2170 mm and $x = 2910$ mm. At $x = 2170$ mm the profile has lost it fullness due to the APG and can no longer withstand the pressure gradient. The flow separates at $x = 2280$ mm and reattaches at $x = 2780$ mm. Although stretched in the wall normal direction, the reattaching profile resembles the profile at the position of separation.

Backflow

The backflow coefficient χ is defined as the fraction of time the flow travels in the upstream direction. Since the flow field is measured by PIV, χ is really the fraction of image-pairs with negative U–velocity. Figure 3 shows how the χ profile develops through the separation bubble.

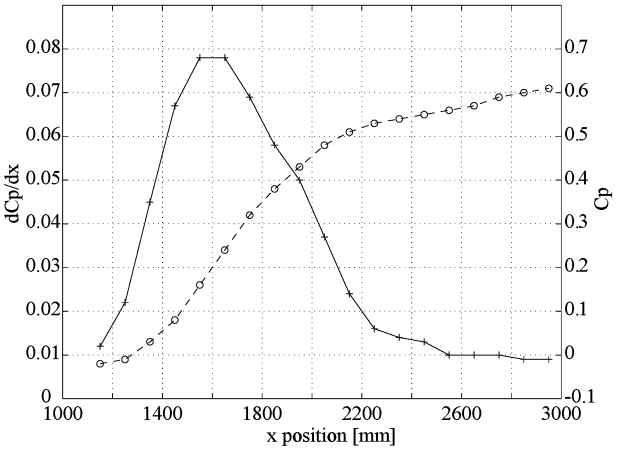

Figure 2: Wall static pressure distribution and pressure gradient on test plate.

In this experiment the line of separation is defined as the x position where the wall value of the backflow coefficient χ_w is 50 %. Dengel & Fernholz (1990) have shown that the line where $\chi_w = 50$ % coincides with the line of zero skin friction. This is valid both at separation and reattachment. In this case the wall value is actually measured 1.5 mm from the wall because of the PIV image resolution.

Although this experiment resembles the one described by AMK (2005a), here the region of $\chi_w > 50$ % is much larger. At the point of maximum thickness of the separated region χ is greater than 0.5 up to approximately $y = 15$ mm.

Integral parameters

The mean flow profiles were used to calculate the displacement thickness δ_1 and the momentum loss thickness δ_2,

$$\delta_1 = \int_0^\delta \left(1 - \frac{U(y)}{U_e}\right) dy \tag{2}$$

$$\delta_2 = \int_0^\delta \frac{U(y)}{U_e}\left(1 - \frac{U(y)}{U_e}\right) dy \tag{3}$$

Their downstream development is shown in figure 4. The form factor $H_{12} = \delta_1/\delta_2$ is shown i figure 5. Before separation δ_2 is almost constant and δ_1 is increasing rapidly, giving an increasing H_{12}. After separation the rate of increase in δ_1 is slightly reduced and δ_2 is starting to increase as well. This reduces the rate of increase in H_{12} and from about x = 2550 mm H_{12} starts to decrease. At the position of mean separation we find that H_{12} is 3.7. This is more than the $H_{12,sep}$ = 2.85 measured by Dengel & Fernholz (1990) and $H_{12,sep}$ = 3.45 estimated by Angele (2003). The shape of the mean velocity profile at the position of reattachment look similar to the separating one, but H_{12} has risen to 4.1.

According to Dengel & Fernholz (1990) the relation between χ_w and H_{12} should be linear. In this experiment this is not the case. A reason for this could be that they measured χ_w using a pulsed wire probe only 0.03 mm above the wall,

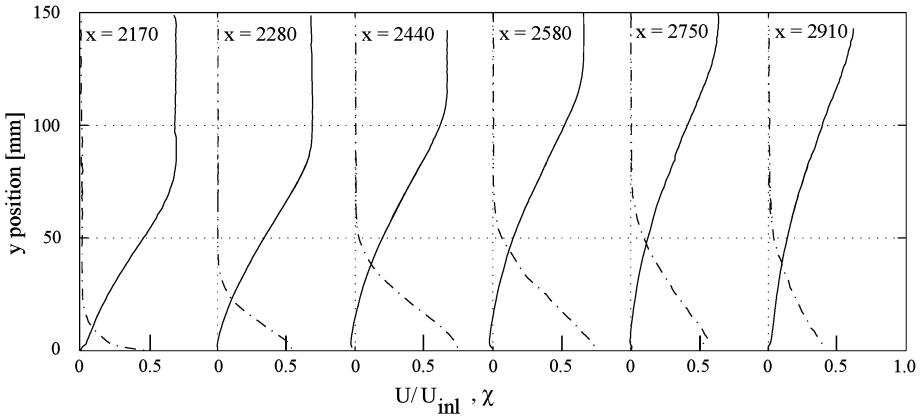

Figure 3: Mean velocity profiles and profiles of the reverse-flow parameter χ at different x positions.

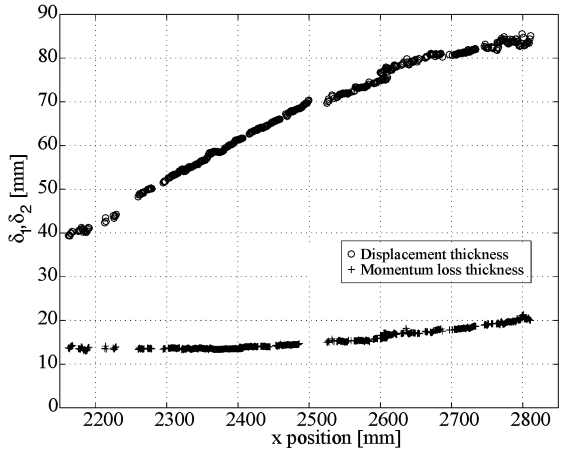

Figure 4: Downstream development of the displacement thickness δ_1 and momentum loss thickness δ_2

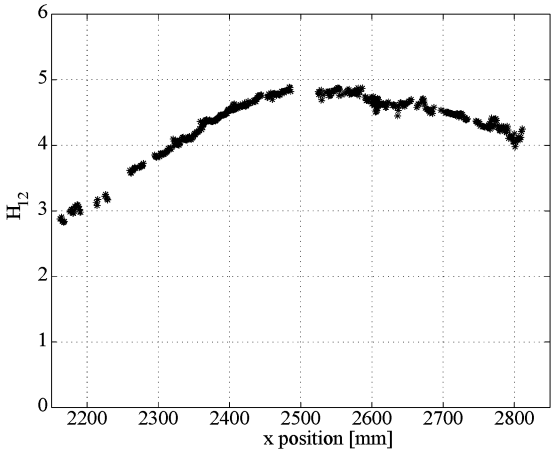

Figure 5: Downstream development of the shape factor $H_{12} = \delta_1/\delta_2$.

.

whereas the resolution near the wall obtained using PIV is not as good. Also their test section is axi-symmetric, while the one used here is rectangular in cross section.

CONTROLLED CASE

Vortex generators

In order to control the separation bubble simple vortex generators were used to create pairs of counter-rotating vortices near the wall. Table 1 summarizes the geometry of the VGs used. See figure 6 for definitions. The blade angle is 15° and the design criteria follows what Pearcy (1961) has suggested. Figure 7 shows a schematic of the generated vortices and where they induce outflow and inflow in the wall normal direction.

Although no direct measurements of the generated circulation were made it can be estimated as

$$\Gamma = \frac{Z}{D} h U \tag{4}$$

where U is the mean velocity at $x = x_{VG}$ and $y = h$. The estimation is very rough but makes it possible to rank the different VG configuration in terms of circulation generated. To our knowledge this procedure of classification was first used by AMK (2005a).

The circulation is varied by means of changing the VG absolute height and by varying the x position and thereby changing the relative height to the boundary layer thickness. The smallest VG configuration tested is $h/\delta = 0.1$ and the circulation created is $\Gamma = 0.5$. For the largest VGs Γ is approximately ten times more, *i.e.* $\Gamma = 4.7$.

Mean flow results

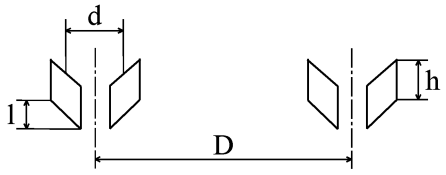

Figure 6: VG geometry. The flow direction is into the picture.

Table 2: Description of the VG configurations used in the experiment.

x_{VG}(mm)	$\frac{x_{sep}-x_{VG}}{h}$	$H_{12,\Gamma=0}$	U_∞(m/s)	h (mm)	h/δ	h/δ_1	Γ
1100	66	1.4	26.5	18	0.95	5.4	4.7
1600	38	1.6	22.5	18	0.53	2.2	3.3
2000	16	2.0	20.5	18	0.30	1.0	2.0
2000	28	2.0	20.5	10	0.17	0.6	0.7
2000	47	2.0	20.5	6	0.10	0.3	0.6

Table 1: Physical dimensions of the VG sets used in the experiment.

h (mm)	d (mm)	l (mm)	D (mm)	l/h	D/h	Z/D
6	12.5	18	50	3	8.33	15
10	21	30	83	3	8.33	9
18	37.5	54	150	3	8.33	5

All comparisons of the effect of the different VG configurations are made at $x = 2500$ mm since this is the position of maximum backflow in the uncontrolled case. Figures 8 and 9 shows the streamwise mean velocity profiles $U(y)$ at the spanwise position of inflow and outflow for the different VG configurations. Obviously their z position vary depending on the VG size and hence spanwise distance between VG pairs. At the position of inflow more U momentum is transported down through the boundary layer and a slightly larger effect of the VGs can be seen compared to the position of outflow. The two weakest VGs of $\Gamma = 0.5$ and $\Gamma = 0.6$ have negligible influence on U. Stepping up to $\Gamma = 2.0$ separation is prevented. The velocity profile might look "weak", with almost the same shape as a reattaching boundary layer, but figures 12 and 13 shows that reverse flow is almost eliminated at the position of inflow and that χ_w is about 0.1 at the position of outflow. This is the most efficient VG configuration for preventing separation in this particular flow case, since the drag generated by these VGs is expected to be less than that generated by the stronger VGs.

The three configurations with 18 mm VGs at different x positions, giving $\Gamma = 2.0$, $\Gamma = 3.3$ and $\Gamma = 4.7$, respectively, were used by AMK (2005a) in the same test section as in the present study. The only difference is the stronger pressure gradient causing a larger separation bubble in the present case. Compared to their results the present data shows less difference in the mean velocity profiles between the position of inflow and the position of outflow, *i.e.* the boundary layer is closer to a two dimensional state.

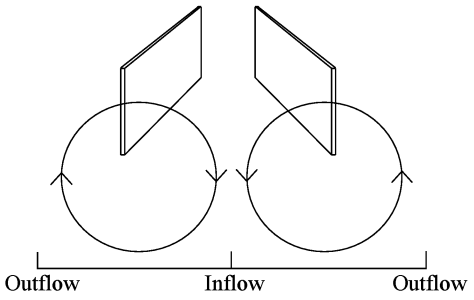

Figure 7: Streamwise vortices downstream of a vortex generator. The position of outflow and tyhe position of inflow is indicated. The flow is out of the picture.

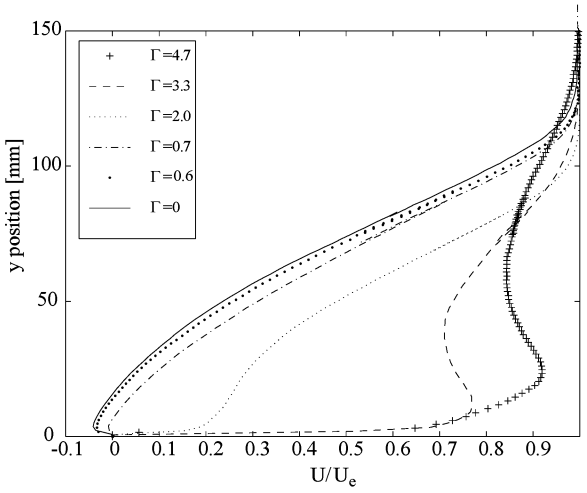

Figure 8: Streamwise mean velocity for different VGs at the spanwise position of inflow at $x = 2500$ mm.

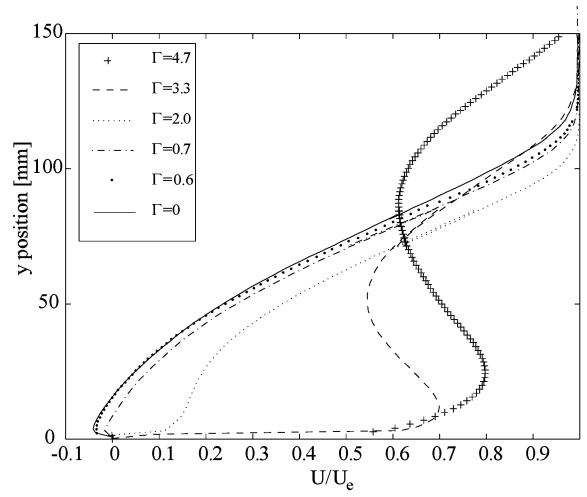

Figure 9: Streamwise mean velocity for different VGs at the spanwise position of outflow at $x = 2500$ mm.

At $\Gamma = 3.3$ and $\Gamma = 4.7$ the U profiles are clearly S-shaped with a negative velocity gradient region between the outer and inner part of the boundary layer. At the position of in-

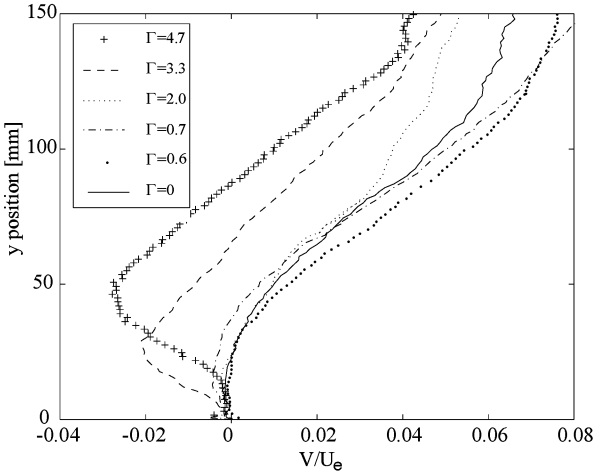

Figure 10: Wall normal mean velocity for different VGs at the spanwise position of inflow at $x = 2500$ mm.

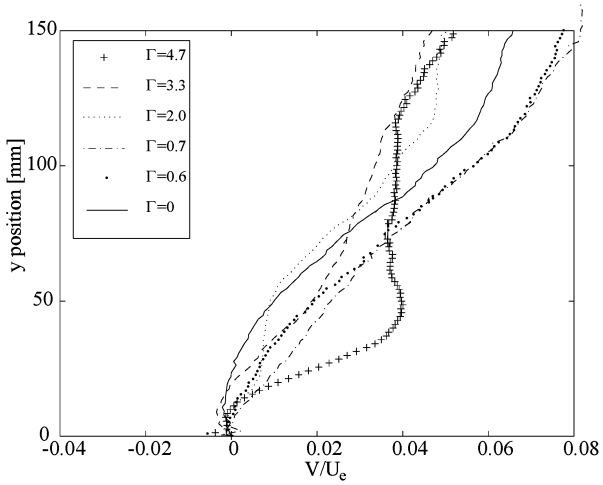

Figure 11: Wall normal mean velocity for different VGs at the spanwise position of outflow at $x = 2500$ mm.

flow both show larger mean velocity gradients than a ZPG boundary layer. For $\Gamma = 4.7$ the profile is almost square. For both the strong profiles the vortices makes the boundary layer substantially thicker. This effect is not observed for $\Gamma \leq 2.0$.

The wall normal mean velocity profiles in figures 10 and 11 are wiggly due to peak-locking. Since the V component is less than a tenth of the U component the accuracy of the V data is worse. But as expected the $V(y)$ profiles for $\Gamma = 3.3$ and 4.7 have a large negative peak near the wall at the position of inflow. The other curves show the same tendency, but less clearly. At the position of outflow the strongest VG produces a positive peak, while the others do not seem to change the profile much.

Figure 14 shows how the shape factor at $x = 2500$ mm depend on Γ. The two curves represent the spanwise positions of inflow and outflow respectively. A fuller profile and hence a smaller H_{12} is expected at the position of inflow. This can be seen in the figure, where the two curves are slightly shifted

There seems to be almost a linear relationship between H_{12} and Γ in the interval $0.5 \leq \Gamma \leq 3.3$, though this might be an

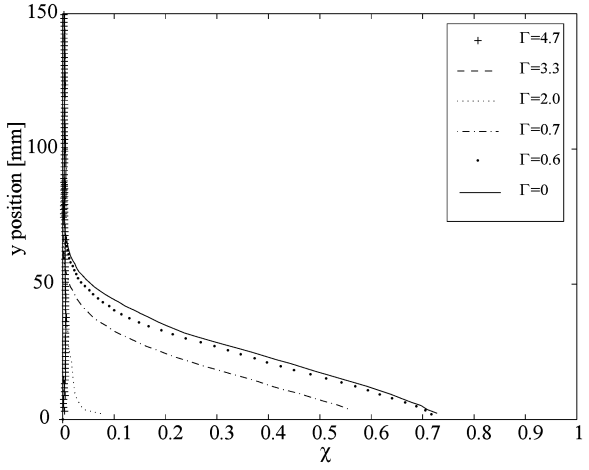

Figure 12: χ for different VGs at the spanwise position of inflow at $x = 2500$ mm.

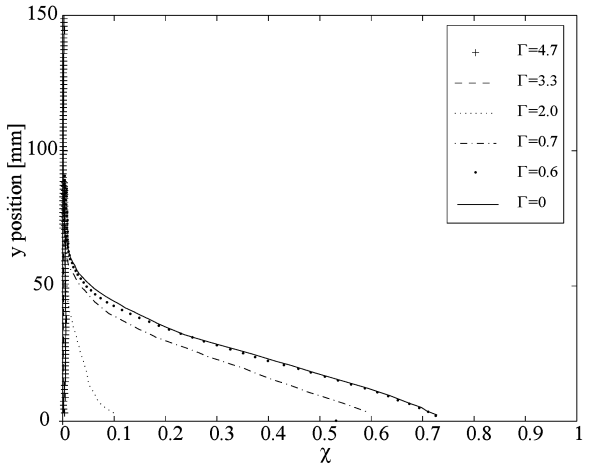

Figure 13: χ for different VGs at the spanwise position of outflow at $x = 2500$ mm.

effect of too few data points.

CONCLUSION

The classification of VGs according to the generated circulation, introduced by AMK (2005a), works well to rank the strength of VGs of different heights and streamwise positions.

In the present experiment submerged vortex generators, with $h/\delta = 0.1$–0.2, placed 30–50 VG heights upstream of the baseline separation location had negligible effect on separation. Earlier studies (Lin et al., 1989) indicating that submerged VGs performs well have been carried out with the VGs applied in a fuller boundary layer of lower H_{12}. In this case a more upstream position would definitively be beneficial. Also, as mentioned by Lin (2000), because of their substantially reduced height, compared to conventional VGs, device parameters such as blade angle and length to height ratio should be increased.

Compared to the earlier study (AMK, 2005a) of VGs controlling a boundary layer on the verge of separation (or with

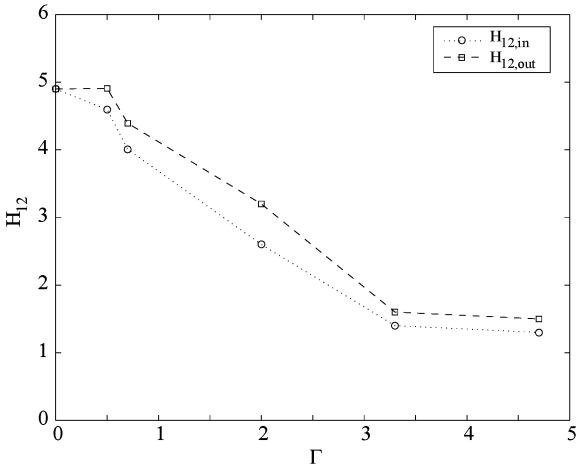

Figure 14: The shape factor plotted against Γ.

a very thin separated region) in the baseline case the present data exhibits a more two dimensional flow field when applying VGs.

ACKNOWLEDGMENTS

The authors thank Scania CV AB for the financial support of this investigation. Olle Törnblom gave valuable data evaluation help. Fruitful discussions and comments by Dr Angele are highly acknowledged.

REFERENCES

Angele, K.P. 2003 Experimental studies of turbulent boundary separation and control. PhD-thesis, Dept. Mechanics, KTH.

Angele, K.P. and Muhammad-Klingmann, B. 2005a The effect of streamwise vortices on the turbulence structure of a separating boundary layer. *Eur. J. Mech./Fluids* (accepted).

Angele, K.P. and Muhammad-Klingmann, B. 2005b A simple model for the effect of peak-locking on the accuracy of boundary layer turbulence statistics in digital PIV. *Exp. Fluids*, vol. 38, pp.341–347.

Darabi, A. and Wygnanski, I. 2004 Active management of naturally separated flow over a solid surface. Part 1. The forced reattachment process. *J. Fluid Mech.* vol. 510, pp. 105–129

Darabi, A. and Wygnanski, I. 2004 Active management of naturally separated flow over a solid surface. Part 2. The separation process. *J. Fluid Mech.* vol. 510, 131–144.

Gad-el-Hak, M. and Bushnell, D. 1991 Status and outlook of flow separation control. *AIAA Paper 91-0037.*

Glezer, A. and Amitay, M. 2002 Synthetic jets. *Annu. Rev. Fluid Mech.* vol. 34, 503–529.

Häggmark, C. 2000 Investigations of disturbances developing in a laminar separation bubble flow. PhD-thesis, Dept. Mechanics, KTH.

Lin, J.C. 2000 review of research on low-profile vortex generators to control boundary-layer separation. *Prog. In Aerospace Sci.* vol. 38, 389–420.

Lin, J.C., Howard, F.G. and Selby, G.V. 1989 Turbulent flow separation control through passive techniques. *AIAA Paper 89-0976.*

Lin, J.C., Howard, F.G. and Bushnell, D.M. 1990 Investigation of several passive and active methods for turbulent flow separation control. *AIAA Paper 90-1598.*

Lindgren, B. and Johansson, A.V. 2004 Evaluation of a new wind-tunnel with expanding corners. *Exp. Fluids*, vol. 36, 197–203.

Pearcy, H.H. 1961 *Shock-induced separation and its prevention by design and boundary-layer control. In Boundary Layer and Flow Control, its Principle and Application, Vol 2, Edited by G.V. Lachmann.* Pergamon press, Oxford, England.